Available online at www.sciencedirect.com
SCIENCE DIRECT®
Journal of Computational Physics 191 (2003) 1–17
JOURNAL OF COMPUTATIONAL PHYSICS
www.elsevier.com/locate/jcp

Remeshed smoothed particle hydrodynamics for the simulation of laminar chemically reactive flows

A.K. Chaniotis [a,*], C.E. Frouzakis [b], J.C. Lee [b,1], A.G. Tomboulides [b,2], D. Poulikakos [a,*], K. Boulouchos [b]

[a] *Institute of Energy Technology, Laboratory of Thermodynamics in Emerging Technologies, ETH Zentrum, Zürich, Switzerland*
[b] *Institute of Energy Technology, Aerothermochemistry and Combustion Systems Laboratory, ETH, Zürich, Switzerland*

Received 8 January 2003; received in revised form 19 May 2003; accepted 6 June 2003

Abstract

We present an extension of the remeshed smooth particle hydrodynamics (RSPH) method for the simulation of chemically reactive flows. The governing conservation equations are solved in a Lagrangian fashion, while particle locations, which are distorted by the flow, are periodically re-initialized (remeshed) on a grid. The RSPH implementation is employed for the simulation of a hydrogen/air opposed-jet burner with detailed chemistry and transport. The effect of particle number (resolution), compressibility (Mach number) and outflow boundary condition (length of the domain) on the solution are considered. The RSPH computational results are compared with numerical results obtained by a spectral element implicit scheme and by a one-dimensional code. It is shown that RSPH provides a flexible and accurate alternative for the numerical simulation of chemically reacting flows.

1. Introduction

Grid-based approaches (e.g., finite element, finite difference, finite volume and spectral methods) are used extensively for the simulation of reacting flows [1]. Lagrangian methods have a marked advantage in convection-dominated flows, where the major contribution of the non-linear convection term can be computed exactly. Unfortunately, they are confronted with a number of problems, ranging from the difficulty in extending the method to multidimensional flows [2], to difficulties in including heat release [3–5], an essential feature of most reacting flows. Substantial efforts have been made to extend Lagrangian particle methods for the simulation of reacting flows. From the purely mathematical point of view, the

* Corresponding authors. Present address: ETH Zentrum, IET, LTNT, Sonneggstrasse 3, Zürich CH-8092, Switzerland. Tel.: +41-1-63-22-435; fax: +41-1-63-21-176 (D. Poulikakos). Tel.: +41-1-63-23-170; fax: +41-1-63-21-176 (A.K. Chaniotis).
E-mail addresses: chaniotis@ltnt.iet.mavt.ethz.ch (A.K. Chaniotis), poulikakos@ltnt.iet.mavt.ethz.ch (D. Poulikakos).
[1] Present address: Combustion Research Facility, Sandia National Laboratories, P.O. Box 969, Livermore, CA 94551-0969, USA.
[2] Present address: Laboratory of Thermodynamics and Internal Combustion Engines, Department of Energy Resource Management and Engineering, Aristotle University of Thessaloniki, Greece.

0021-9991/$ - see front matter
doi:10.1016/S0021-9991(03)00302-4

Lagrangian representation of the transport equations that describe a chemically reacting flow is not complicated. However, the development of an appropriate solution procedure capable of solving these transport equations within the Lagrangian frame is not a simple task.

Vortex methods have been successfully applied in the simulation of incompressible flows. When extending vortex methods to reacting flows, there are two general ways [6] by which the effect of chemistry can be taken into account: interface methods, and direct Lagrangian methods. In interface methods, chemical reactions are assumed to occur within a narrow zone. These approaches are best suited for simulating unsteady premixed flames. The chemical reaction effect is included by adding a thermal expansion and baroclinic torque term in the continuity and vorticity transport equations, respectively [3,4]. Direct Lagrangian methods were developed as an extension of the transport element method [7,8] to the simulation of unsteady reacting flows. No assumptions are made with respect to the structure and topology of the reaction zone, however; these models are not considered ready to study 3-D reacting flows (compared to conventional combustion modeling techniques) [6]. The method has been applied successfully in fundamental aspects of reacting flows (e.g., reacting mixing layer simulations), mainly with a single-step reaction of finite or infinite rate. Direct Lagrangian methods can be extended to systems with more species, but are restricted to equal diffusivities of the species [9]. The coupling errors that are caused by the combination of convection and other physical processes in reacting vortex methods are not well understood, and may lead to incorrect solutions [10]. The direct Lagrangian methods are regarded more often as a large eddy simulation techniques [6] using modeling mechanisms to account for small-scale transport [3,4,7–9,11,12].

Another particle method that has been successfully applied in the simulation of systems with reactions is the particle-in-cell (PIC) method [13]. Convective transport is solved using particles, while other processes are solved on a grid. However, PIC with reaction is computationally expensive compared to same order grid-based methods [14].

To the best of our knowledge, the Smooth Particle Hydrodynamics (SPH) method has not been applied to the simulation of reacting flows. In this paper, the remeshed SPH implementation (RSPH) presented in [15] is extended for the simulation of chemically reacting flows. All the transport equations and terms are solved in a Lagrangian fashion simultaneously (without linearization or background grid-based differentiation). The resulting algorithm retains all the computational features of particle methods: adaptivity, robustness, no convection-related stability limitations, and, because of the local character of particle interactions, it can be efficiently parallelized in a straightforward way. In addition, it can be easily extended to include multi-phase effects.

The present paper is organized as follows: in Section 2, we outline the governing equations and present their particle discretization. In Section 3, the method is applied to the simulation of a two-dimensional hydrogen/air opposed-jet burner with detailed chemistry and transport. The effects of resolution (number of particles), compressibility (Mach number), and outflow boundary condition (length of the domain) on the solution are also discussed in the same section.

2. Governing equations and RSPH methodology

2.1. Governing equations

The motion of a viscous, heat conducting, reacting, and compressible medium is described by the continuity, momentum, energy, and species concentration equations. For a multi-component, calorically perfect gas the conservation equations are [16]:

$$\frac{\mathrm{D}\rho}{\mathrm{D}t} = -\rho \frac{\partial u_i}{\partial x_i}, \tag{1}$$

$$\rho \frac{\mathrm{D}u_i}{\mathrm{D}t} = -\frac{\partial p}{\partial x_i} + \frac{\partial \tau_{ij}}{\partial x_j}, \tag{2}$$

$$\rho c_{\mathrm{v}} \frac{\mathrm{D}T}{\mathrm{D}t} = -p\frac{\partial u_i}{\partial x_i} + \tau_{ij}\frac{\partial u_i}{\partial x_j} + \dot{Q} - \frac{\partial q_i}{\partial x_i}, \tag{3}$$

$$\frac{\mathrm{D}\rho Y_s}{\mathrm{D}t} = -\rho Y_s \frac{\partial u_i}{\partial x_i} - \frac{\partial \rho Y_s V_{s_i}}{\partial x_i} + \dot{R}_s, \tag{4}$$

where x_i, u_i are the components of the position and the velocity vector, respectively, ρ the density, p the pressure, T the temperature, μ the viscosity, k the thermal conductivity, c_{v} the mean specific heat at constant volume, $\dot{Q}$ the heat release rate, s the species index, c_{p_s} the specific heat at constant pressure of species s, Y_s the mass fraction of species s, $\dot{R}_s$ the mass rate of production of species s, and V_{s_i} the diffusion velocity of species s. In these equations, $\mathrm{D}/\mathrm{D}t$ is the material derivative:

$$\frac{\mathrm{D}}{\mathrm{D}t} = \frac{\partial}{\partial t} + u_i \frac{\partial}{\partial x_i}, \tag{5}$$

and Einstein's index notation is used for vectors and tensors. Viscous stresses, τ_{ij}, and the heat flux vector are:

$$\tau_{ij} = \mu\left(\frac{\partial u_i}{\partial x_j} + \frac{\partial u_j}{\partial x_i} - \frac{2}{3}\delta_{ij}\frac{\partial u_k}{\partial x_k}\right), \tag{6}$$

$$q_i = -k\frac{\partial T}{\partial x_i} + \rho \sum_{s=1}^{\text{Species}} c_{\mathrm{p}_s} T Y_s V_{s_i}. \tag{7}$$

The heat flux vector q_i (in Eq. (7)) contains the heat conduction and thermal diffusion (Soret) effect. The influence of species diffusion on thermal transport (Dufour effect) is of minor importance in combustion simulations and will be neglected [17]. Radiation through a fluid containing combustion products depends on the temperature and composition throughout the entire field. Except in sooting flames, radiation is usually a small fraction of the total heat flow and is neglected in combustion simulations of "thin" flames, in order to avoid the complexities associated with its description. Neglecting the thermal diffusion velocity (which is significant only for low molecular weight species), the diffusion velocities, $V_{s_i}^{\mathrm{C}}$, can be written in the classical Fickian form [16]:

$$V_{s_i}^{\mathrm{C}} = -\frac{1}{X_s} D_s \frac{\partial X_s}{\partial x_i}, \tag{8}$$

where X_s the mole fraction, and D_s the mixture-average diffusion coefficient of species s. Mixture-average diffusion coefficients are approximations [18], and do not guarantee that the net species diffusion flux is zero (i.e., $\sum_{s=1}^{\text{Species}} Y_s \boldsymbol{V}_s = 0$), and, therefore, conservation of mass (i.e., $\sum_{s=1}^{\text{Species}} Y_s \neq 1$). One approach to correct this [19] is to add a correction factor, $\boldsymbol{V}_{\mathrm{c}}$, so that $\boldsymbol{V}_s = \boldsymbol{V}_s^{\mathrm{C}} + \boldsymbol{V}_{\mathrm{c}}$. $\boldsymbol{V}_{\mathrm{c}}$ is independent of species, but spatially varying, and is defined as:

$$\boldsymbol{V}_{\mathrm{c}} = -\sum_{s=1}^{\text{Species}} Y_s \boldsymbol{V}_s^{\mathrm{C}}. \tag{9}$$

All thermodynamic and transport properties depend on temperature and mixture composition [18,20].

The system of differential Eqs. (1)–(4) is closed with the equation of state for an ideal gas

$$p = \rho R T, \tag{10}$$

where R is the gas constant.

The non-dimensional variables are obtained from the dimensional variables as follows:

$$x_i^* = \frac{x_i}{L_0}, \quad \rho^* = \frac{\rho}{\rho_0}, \quad t^* = \frac{t}{L_0/U_0}, \quad u_i^* = \frac{u_i}{U_0}, \quad T^* = \frac{T}{T_0},$$

$$p^* = \frac{p}{\rho_0 R T_0}, \quad \mu^* = \frac{\mu}{\mu_0}, \quad k^* = \frac{k}{k_0}, \quad c_{\mathrm{v}}^* = \frac{c_v}{c_{\mathrm{v}0}}, \quad c_{\mathrm{p}_s}^* = \frac{c_{\mathrm{p}_s}}{c_{\mathrm{v}0}\gamma}, \tag{11}$$

$$\dot{Q}^* = \frac{\dot{Q}}{\rho_0 c_{\mathrm{v}0} T_0 U_0/L_0}, \quad D_s^* = \frac{D_s}{D_0}, \quad \dot{R}^* = \frac{\dot{R}_s}{\rho_0 U_0/L_0},$$

where the superscript * and the subscript $_0$ indicate the non-dimensional and reference quantities, respectively. The quantities $L_0, \rho_0, U_0, T_0, \mu_0, k_0, D_0$ and $c_{\mathrm{v}0}$ denote the characteristic length, density, velocity, temperature, viscosity, thermal conductivity, diffusion coefficient, and specific heat at constant volume, respectively. In non-dimensional form, the system of governing equations (neglecting the Soret effect for comparison purposes in Eq. (7)) can be written:

$$\frac{\mathrm{D}\rho^*}{\mathrm{D}t^*} = -\rho^* \frac{\partial u_i^*}{\partial x_i^*}, \tag{12}$$

$$\rho^* \frac{\mathrm{D}u_i^*}{\mathrm{D}t^*} = -\frac{1}{M^2\gamma}\frac{\partial p^*}{\partial x_i^*} + \frac{1}{Re}\frac{\partial \tau_{ij}^*}{\partial x_j^*}, \tag{13}$$

$$\rho^* c_{\mathrm{v}}^* \frac{\mathrm{D}T^*}{\mathrm{D}t^*} = -(\gamma-1)p^*\frac{\partial u_i^*}{\partial x_i^*} + \frac{M^2\gamma(\gamma-1)}{Re}\tau_{ij}^*\frac{\partial u_i^*}{\partial x_j^*} + \dot{Q}^* + \frac{\gamma}{RePr}\frac{\partial}{\partial x_i^*}\left(k^*\frac{\partial T^*}{\partial x_i^*}\right), \tag{14}$$

$$\frac{\mathrm{D}\rho^* Y_s}{\mathrm{D}t} = -\rho^* Y_s \frac{\partial u_i^*}{\partial x_i^*} + \frac{1}{Pe}\frac{\partial}{\partial x_i^*}\left(\rho^* Y_s \frac{D_s^*}{X_s}\frac{\partial X_s}{\partial x_i^*}\right) - \frac{1}{Pe}\sum_{ss=1}^{\text{Species}}\left(\frac{\partial}{\partial x_i^*}\left(\rho^* Y_s \frac{D_{ss}^*}{X_{ss}}\frac{\partial X_{ss}}{\partial x_i^*}\right)\right) + \dot{R}_s^*, \tag{15}$$

$$p^* = \rho^* T^*, \tag{16}$$

$$\tau_{ij}^* = \mu^*\left(\frac{\partial u_i^*}{\partial x_j^*} + \frac{\partial u_j^*}{\partial x_i^*} - \frac{2}{3}\delta_{ij}\frac{\partial u_k^*}{\partial x_k^*}\right). \tag{17}$$

The dimensionless numbers that appear in the equations are the Reynolds number, Re, the Mach number, M, the Prandtl number, Pr, and the Peclet number, Pe:

$$Re = \frac{\rho_0 U_0 L_0}{\mu_0}, \quad M^2 = \frac{U_0^2}{\gamma R T_0}, \quad Pr = \frac{\mu_0 \gamma c_{\mathrm{v}0}}{k_0}, \quad Pe = \frac{U_0 L_0}{D_0}, \tag{18}$$

where γ is the ratio of the specific heat capacities.

The set of equations presented above includes acoustic interactions and compressibility effects, as well as heating due to viscous dissipation. Body forces (e.g., gravitational) and thermal radiation effects are neglected.

2.2. Numerical method

The numerical method used in the present study is based on the Lagrangian formulation of the governing equations. The flow quantities are discretized into particles using the Smooth Particle Hydrodynamics technique [21–23]. Each particle α is associated with a mass m_α, density ρ_α, velocity $(u_i)_\alpha$, viscosity μ_α, pressure p_α, temperature T_α, thermal conductivity k_α, mass fraction $(Y_s)_\alpha$, heat release rate $\dot{Q}_a$, reaction rate $(\dot{R}_s)_\alpha$, and position $(x_i)_\alpha$ and all the necessary thermodynamic quantities involved in Eqs. (1)–(10). The particles move in a Lagrangian fashion according to the formula:

$$\frac{\mathrm{d}x_i}{\mathrm{d}t} = u_i. \tag{19}$$

All the quantities are interpolated on the particle locations and all the flow quantities can be reconstructed by a linear superposition of the flow quantities carried by the particles as weighed by a smooth interpolation kernel.

The gradient operator of a scalar quantity A for the particle α can be written [15]:

$$\langle \nabla A \rangle_a = \sum_b V_b (A_b - A_a) \nabla W(r_a - r_b, h) \tag{20}$$

and the second-order derivative for the location of the α particle can be written [15]:

$$\left\langle \frac{\partial^2 A}{\partial x_i x_j} \right\rangle_a = \sum_b V_b (A_b - A_a) \cdot \frac{\partial^2}{\partial x_i x_j} W(r_a - r_b, h), \tag{21}$$

where $\langle \cdot \rangle_a$ denotes a quantity associated with particle α, where A_i, V_i $(i = \alpha, b)$ are the values of the scalar and the volume of particle i, W is the interpolation kernel, and h is a scaling variable with dimension of length.

The choice of the interpolation kernel is the core of the method. Most SPH simulations use splines (cubic, quartic and quintic) [23–25]. In our implementation the quartic spline is used [26]. It is constructed from three B-splines requiring kernel and its first, second and third derivative to be continuous. To maintain the particle resolution (which can be distorted by the flow), and ensure to accurate evaluation of second derivatives, particles are periodically re-initialized (remeshed) on a uniform grid by high-order, moment-conserving schemes [27,28]. Remeshing introduces numerical diffusion, but on the other hand eliminates problems associated with particle distortion. It must be noted that the added dissipation induced by remeshing is proportional to the gradients of the flow which would have been introduced by particle distortion if remeshing was not applied. With remeshing, gradients of the field variables remain small. A detailed description of the algorithm can be found in [15].

The resulting discretized equations are (more details in [15,21,22]):

$$\frac{\mathrm{D}\rho_a}{\mathrm{D}t} = -\rho_a \sum_b V_b \left(\vec{u}_b - \vec{u}_a \right) \cdot \nabla_a W(r_a - r_b, h), \tag{22}$$

$$\left\langle \rho \frac{\mathrm{D}u}{\mathrm{D}t} \right\rangle_a = -\left\langle \frac{\partial p}{\partial x} \right\rangle_a + \frac{4}{3} \left\langle \frac{\partial}{\partial x} \mu \frac{\partial u}{\partial x} \right\rangle_a - \frac{2}{3} \left\langle \frac{\partial}{\partial x} \mu \frac{\partial v}{\partial y} \right\rangle_a + \left\langle \frac{\partial}{\partial y} \mu \frac{\partial u}{\partial y} \right\rangle_a + \left\langle \frac{\partial}{\partial y} \mu \frac{\partial v}{\partial x} \right\rangle_a, \tag{23}$$

$$\left\langle \rho \frac{\mathrm{D}v}{\mathrm{D}t} \right\rangle_a = -\left\langle \frac{\partial p}{\partial y} \right\rangle_a + \frac{4}{3} \left\langle \frac{\partial}{\partial y} \mu \frac{\partial v}{\partial y} \right\rangle_a - \frac{2}{3} \left\langle \frac{\partial}{\partial y} \mu \frac{\partial u}{\partial x} \right\rangle_a + \left\langle \frac{\partial}{\partial x} \mu \frac{\partial u}{\partial y} \right\rangle_a + \left\langle \frac{\partial}{\partial x} \mu \frac{\partial v}{\partial x} \right\rangle_a. \tag{24}$$

To take into account the variable viscosity, μ, in an efficient way, the viscous terms are discretized as:

$$\begin{aligned}\left\langle \frac{\partial}{\partial x_i}\mu\frac{\partial u_k}{\partial x_j}\right\rangle_a &= \left\langle \frac{\partial \mu}{\partial x_i}\right\rangle_a \left\langle \frac{\partial u_k}{\partial x_j}\right\rangle_a + \left\langle \mu\frac{\partial^2 u_k}{\partial x_i x_j}\right\rangle_a \\ &= \left(\sum_b V_b(\mu_b-\mu_a)\frac{\partial}{\partial x_i}W(r_a-r_b,h)\right)\left(\sum_b V_b(u_{k,b}-u_{k,a})\frac{\partial}{\partial x_j}W(r_a-r_{b,h})\right) \\ &\quad + \mu_a\sum_b V_b(u_{k,b}-u_{k,a})\frac{\partial^2}{\partial x_i x_j}W(r_a-r_{b,h}).\end{aligned} \tag{25}$$

The two-dimensional version of the energy Eq. (3) reads

$$\begin{aligned}\left\langle \rho c_v\frac{\mathrm{D}T}{\mathrm{D}t}\right\rangle_a &= -\left\langle p\left(\frac{\partial u}{\partial x}+\frac{\partial v}{\partial y}\right)\right\rangle_a + \left\langle \frac{2}{3}\mu\left[\left(\frac{\partial u}{\partial x}-\frac{\partial v}{\partial y}\right)^2+\left(\frac{\partial u}{\partial x}\right)^2+\left(\frac{\partial v}{\partial y}\right)^2\right]\right\rangle_a \\ &\quad + \left\langle \mu\left[\left(\frac{\partial v}{\partial x}-\frac{\partial u}{\partial y}\right)^2\right]\right\rangle_a + \left\langle \dot{Q}\right\rangle_a + \left\langle \frac{\partial}{\partial x}k\frac{\partial T}{\partial x}\right\rangle_a + \left\langle \frac{\partial}{\partial y}k\frac{\partial T}{\partial y}\right\rangle_a.\end{aligned} \tag{26}$$

The compressibility and viscous dissipation term in the energy equation can be easily discretized by using the general formula of Eq. (20).

The derivation of the SPH formulation for the heat diffusion term, allowing for a temperature dependent thermal conductivity, is similar to that of the viscous terms of the momentum equation described above. The final result reads

$$\begin{aligned}\left\langle \frac{\partial}{\partial x_i}\left(k\frac{\partial T}{\partial x_i}\right)\right\rangle_a &= \left\langle \frac{\partial k}{\partial x_i}\right\rangle_a\left\langle \frac{\partial T}{\partial x_i}\right\rangle_a + \left\langle k\frac{\partial^2 T}{\partial x_i^2}\right\rangle_a \\ &= \left(\sum_b V_b(k_b-k_a)\frac{\partial}{\partial x_i}W(r_a-r_b,h)\right)\left(\sum_b V_b(T_b-T_a)\frac{\partial}{\partial x_i}W(r_a-r_b,h)\right) \\ &\quad + k_a\sum_b V_b(T_b-T_a)\frac{\partial^2}{\partial x_i^2}W(r_a-r_b,h).\end{aligned} \tag{27}$$

Finally, the conservation equation of species is written as:

$$\begin{aligned}\left\langle \frac{\mathrm{D}\rho Y_s}{\mathrm{D}t}\right\rangle_a &= -\left\langle \rho Y_s\left(\frac{\partial u}{\partial x}+\frac{\partial v}{\partial y}\right)\right\rangle_a + \left\langle \frac{\partial}{\partial x}\left(\rho Y_s\frac{D_s}{X_s}\frac{\partial X_s}{\partial x}\right)\right\rangle_a + \left\langle \frac{\partial}{\partial y}\left(\rho Y_s\frac{D_s}{X_s}\frac{\partial X_s}{\partial y}\right)\right\rangle_a \\ &\quad - \left\langle \sum_{ss=1}^{\text{Species}}\left(\frac{\partial}{\partial x}\left(\rho Y_s\frac{D_{ss}}{X_{ss}}\frac{\partial X_{ss}}{\partial x}\right)\right)\right\rangle_a - \left\langle \sum_{ss=1}^{\text{Species}}\left(\frac{\partial}{\partial y}\left(\rho Y_s\frac{D_{ss}}{X_{ss}}\frac{\partial X_{ss}}{\partial y}\right)\right)\right\rangle_a + \left\langle \dot{R}_s\right\rangle_a.\end{aligned} \tag{28}$$

Using the general formula of Eq. (20), the first term of the species equation can be easily discretized. The species diffusion terms in (28) that correspond to the diffusion velocity, Eq. (8), and to the correction velocity, Eq. (9), reads:

$$\left\langle \frac{\partial}{\partial x_i}\left(\underbrace{\rho Y_s\frac{D_s}{X_s}}_{A_s}\frac{\partial X_s}{\partial x_i}\right)\right\rangle_a = \left\langle \frac{\partial}{\partial x_i}A_s\right\rangle_a\left\langle \frac{\partial X_s}{\partial x_i}\right\rangle_a + \left\langle A_s\frac{\partial^2 X_s}{\partial x_i^2}\right\rangle_a, \tag{29}$$

$$\left\langle \sum_{ss=1}^{\text{Species}} \frac{\partial}{\partial x_i} \left(\underbrace{\rho Y_s \frac{D_{ss}}{X_{ss}}}_{B_{ss}} \frac{\partial X_{ss}}{\partial x_i} \right) \right\rangle_a = \sum_{ss=1}^{\text{Species}} \left(\left\langle \frac{\partial}{\partial x_i} B_{ss} \right\rangle_a \left\langle \frac{\partial X_s}{\partial x_i} \right\rangle_a + \left\langle B_{ss} \frac{\partial^2 X_s}{\partial x_i^2} \right\rangle_a \right), \tag{30}$$

which can also be expressed in a way similar to Eq. (27). Note that in order to avoid the nested summation and the associated increase in computational cost, the correction velocity is written in vector form.

The diffusion operators (in momentum, energy and species concentrations equations) are written in a general discretized form for variable diffusion coefficients using direct second differentiation of the kernel. The derived formulas are not symmetric and they do not conserve the linear and angular moments algebraically. For constant diffusion coefficients the operators become symmetric and consequently conservative.

3. Results and discussion

The RSPH technique was used for the simulation of a two-dimensional laminar, planar, hydrogen-air opposed-jet burner (Fig. 1). A schematic representation of the geometry used is shown in Fig. 1. For the numerical simulations, only half of the domain is considered. The inflow conditions for both jets are:

$$v = 0, \quad u = u_{\max}\left(1 - \frac{y^2}{B^2/4}\right), \quad T_{\text{inlet}} = 300\,\text{K}, \tag{31}$$

where B is the slot width.

The oxidizer is air (with mole fractions $X_{O_2} = 0.21$, $X_{N_2} = 0.79$) and the fuel is diluted hydrogen ($X_{H_2} = 0.40$, $X_{N_2} = 0.60$). The Reynolds number is defined as

$$Re = \frac{u_{\max}\rho_{\text{oxidizer}}B}{\mu_{\text{oxidizer}}}. \tag{32}$$

The jet width, B, is equal to 0.54 cm. The upper and lower walls are considered isothermal and non-reactive (no-slip, no penetration, $T = 300\,\text{K}$), the outflow conditions are of zero gradient type ($\mathrm{d}u/\mathrm{d}x = \mathrm{d}v/\mathrm{d}x = \mathrm{d}Y_s/\mathrm{d}x = \mathrm{d}T/\mathrm{d}x = 0$), and ambient pressure, while the axis of symmetry is a zero-gradient boundary ($u = \mathrm{d}v/\mathrm{d}x = \mathrm{d}T/\mathrm{d}x = \mathrm{d}\rho/\mathrm{d}x = \mathrm{d}Y_s/\mathrm{d}x = 0$). Unless otherwise noted, the ratio of jet separation distance to jet diameter will be $H/B = 1$, and the domain length will be $L = 3B$.

The numerical simulation of compressible flow requires accurate control of wave reflections from the computational domain. For accurate predictions, it is necessary to eliminate the acoustic waves by a mechanism similar to non-reflecting or absorbing boundary conditions [29] (subsonic inflow, subsonic reacting outflow, adiabatic slip wall). All thermodynamic and transport properties depend on temperature and mixture composition [18,20]. The system of discretized equations are integrated fully implicitly with the ordinary differential equation integrator VODEPK [30].

For the example conditions considered here, $Re = 508.76$ (laminar jets), and $Pr = 0.714$. The actual value of the Mach number is 0.008, corresponding to a practically incompressible flow. In the simulations, in order to avoid the time-step restriction due to acoustic wave propagation, the Mach number is set to 0.05. In our formulation the system of differentials equations becomes stiff when Mach number becomes very small; acoustic waves need to be resolved accurately leading to very small time steps. The detailed chemical mechanism of Yetter et al. [31] involving nine species (O_2, H_2, H, O, OH, H_2O, HO_2, H_2O_2 and N_2) and 21 reversible reactions is employed.

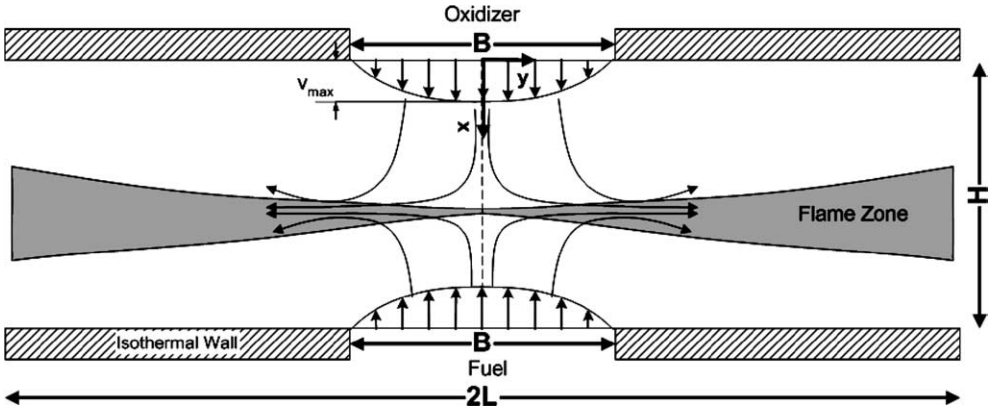

Fig. 1. Geometry of two-dimensional planar opposed-jet diffusion burner.

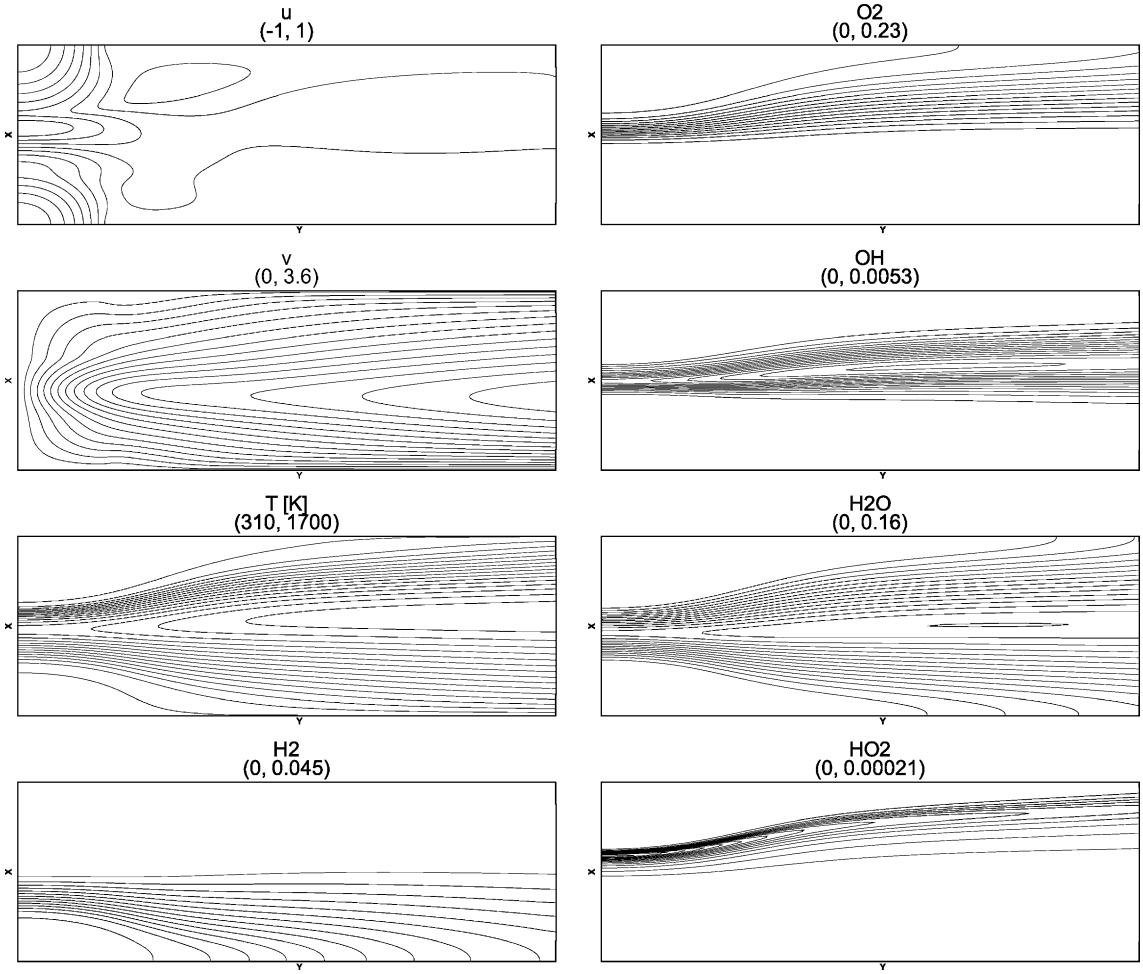

Fig. 2. Isolines of velocities, temperature and representative species mass fractions, from RSPH simulation using 97,200 particles. Sixteen equidistant isolines for each variable covering the range of values shown in parentheses are plotted.

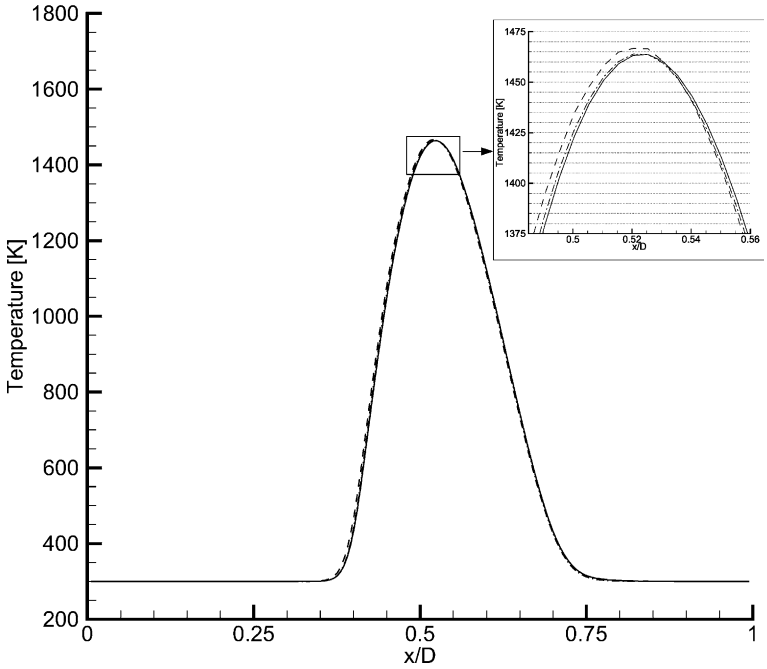

Fig. 3. Temperature profiles along the axis of symmetry obtained with RSPH: (—) 97,200 particles, (- - -) 44,000 particles, (-·-·-) 174,000 particles.

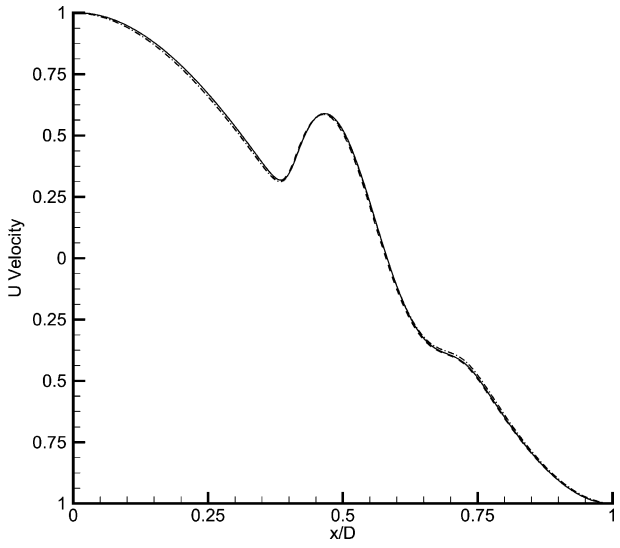

Fig. 4. Axial velocity profiles (non-dimensional) along the axis of symmetry. obtained with RSPH: (—) 97,200 particles, (- - -) 44,000 particles, (-·-·-) 174,000 particles.

For all computed cases, we first obtained the "cold" flow solution, which represents the mixing problem between the fuel and oxidizer jet. The whole ignition process was then simulated by introducing a hot spot around the stagnation plane along the plane of symmetry. The computations then proceeded until all transients died out and the steady state was reached.

Fig. 2 shows the steady-state isocontours of the velocity components, temperature, and representative species, using 97,200 particles (corresponding to 180×540 grid). In order to study the dependence of the solution on the number of particles, simulations using a coarser particle resolution (44,000 particles, corresponding to a 120×360 grid) and a finer particle resolution (174,000 particles, corresponding to a 240×720 grid) were performed. The results of the comparison are shown in Figs. 3–5. The temperature profile along the axis (Fig. 3) shows very good agreement among the three simulations; the difference of the maximum temperature is less than 1%. The flame location and thickness are also in very good agreement. In Fig. 4 the axial velocity plot along the axis of symmetry is shown: the axial velocity profile, as well as the location of the stagnation point is almost identical in all three simulations. Similar behavior can be observed in the species distribution along the symmetry axis in Fig. 5.

As mentioned above, the Mach number was set arbitrarily to 0.05 to avoid a prohibitively restrictive time step. In order to study the effect of Mach number on the solution, we performed simulations for two

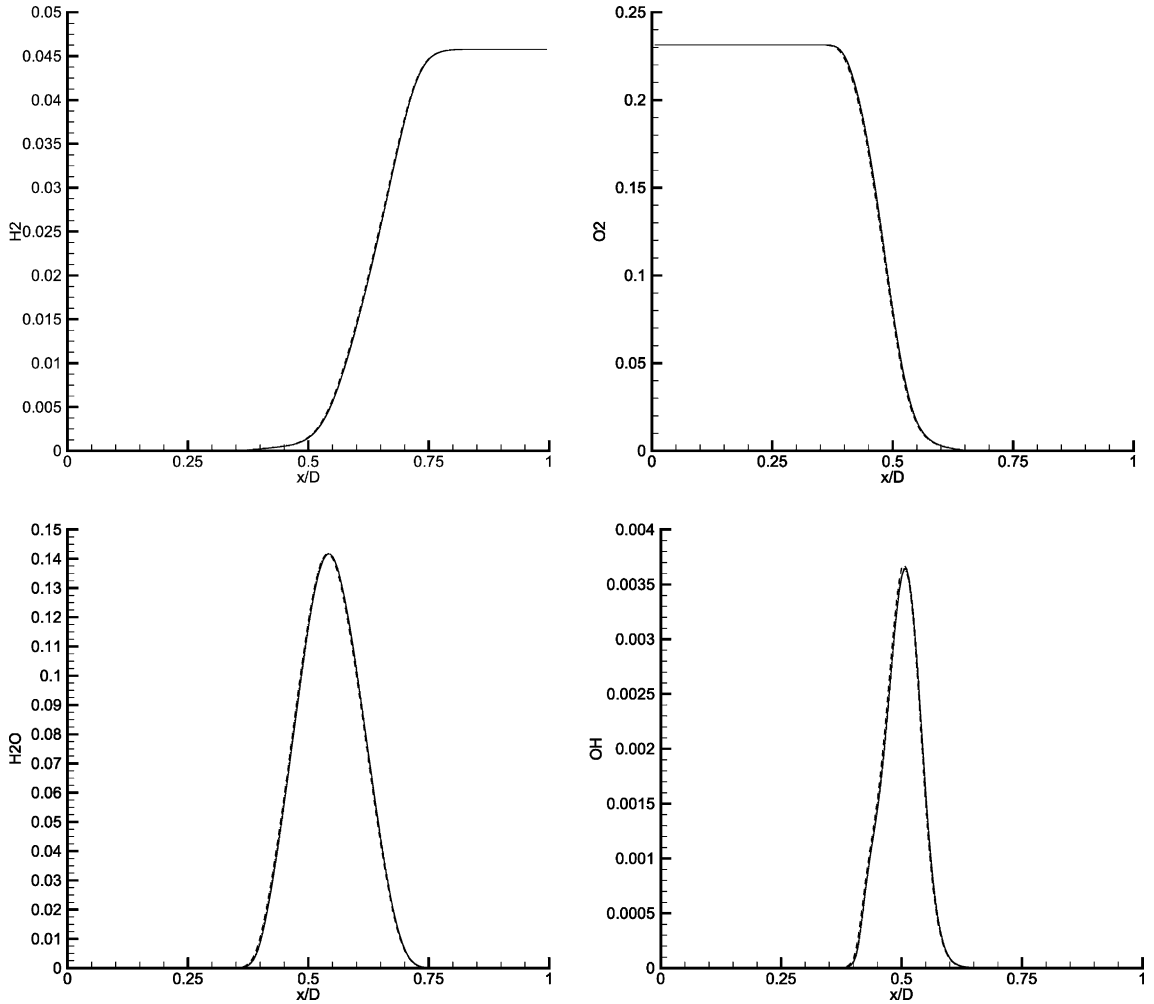

Fig. 5. Mass fraction profiles of H_2, O_2, H_2O and OH along the axis of symmetry obtained with RSPH: (—) 97,200 particles, (- - -) 44,000 particles, (-···-) 174,000 particles.

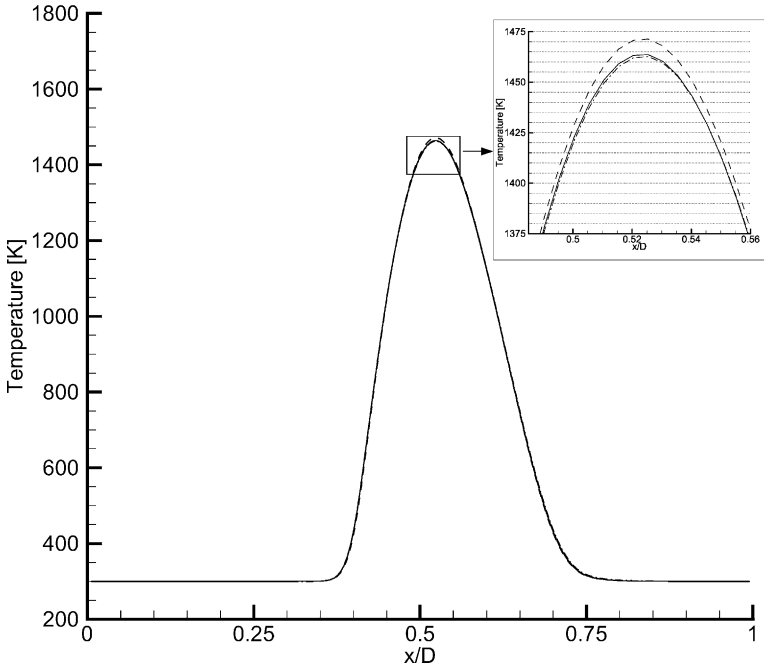

Fig. 6. Temperature profiles along the axis of symmetry for different Mach numbers obtained with RSPH: (—) 97,200 particles with $Ma = 0.05$, (- - -) 97,200 particles with $Ma = 0.1$, (-·-·-) 97,200 particles with $Ma = 0.025$.

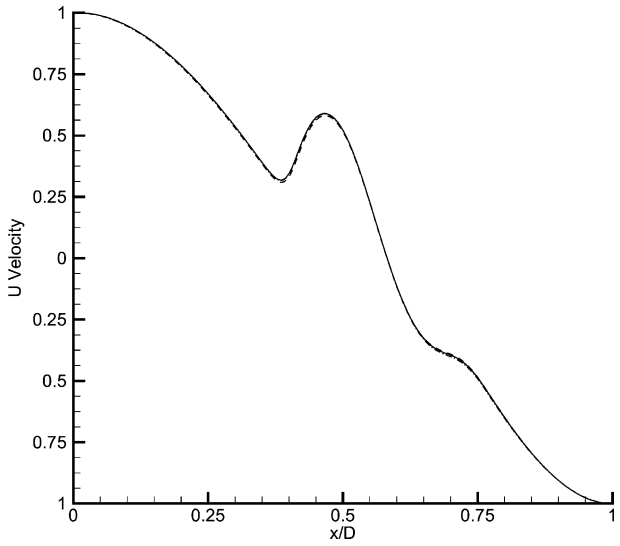

Fig. 7. Axial velocity profiles (non-dimensional) along the axis of symmetry for different Mach numbers obtained with RSPH: (—) 97,200 particles with $Ma = 0.05$, (- - -) 97,200 particles with $Ma = 0.1$, (-·-·-) 97,200 particles with $Ma = 0.025$.

additional values of Ma: one with higher ($Ma = 0.1$) and one with lower ($Ma = 0.025$). As can be seen in Figs. 6–8, for the range considered here, the value of Ma has negligible effect on the solution. The difference in temperature and velocity is less than 1.5%.

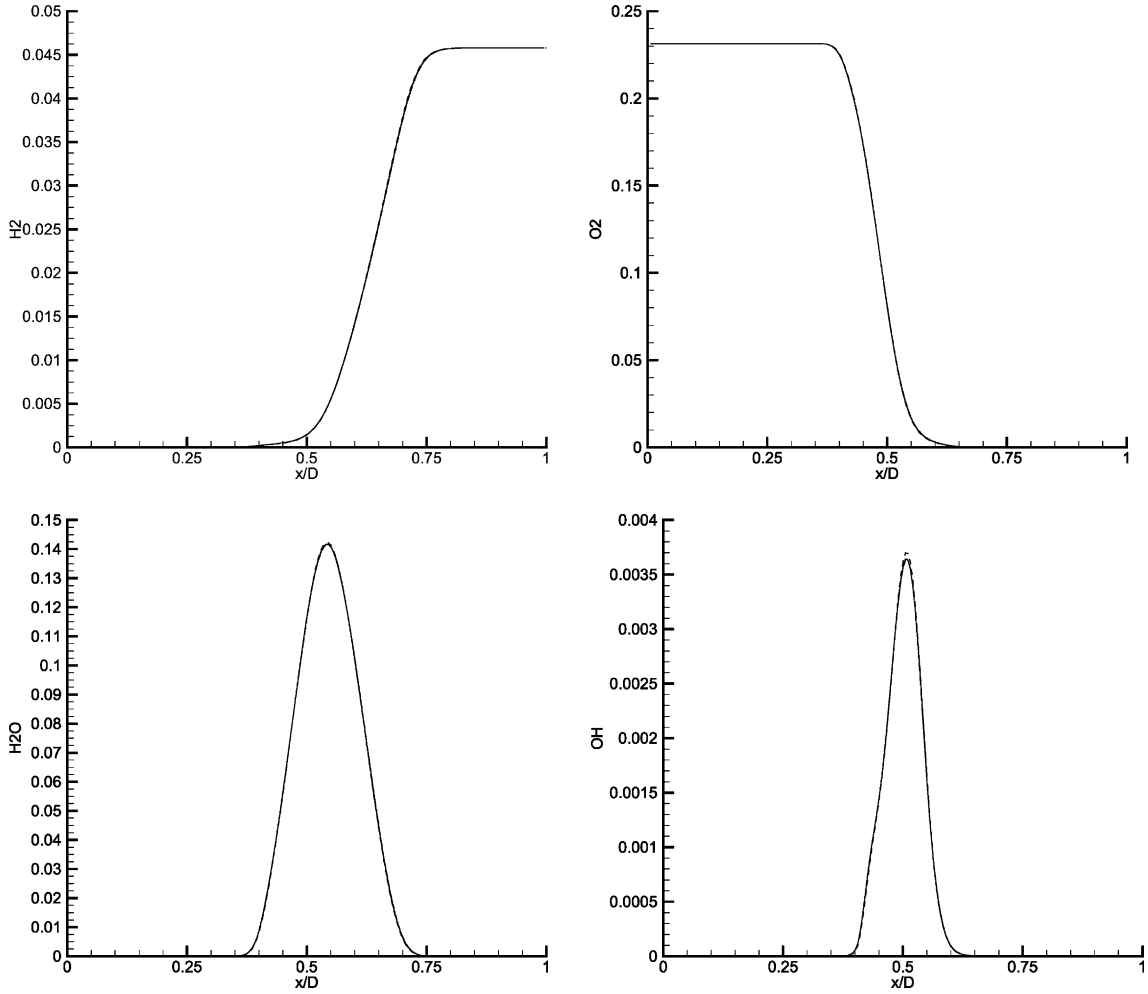

Fig. 8. Mass fraction profiles of H_2, O_2, H_2O and OH along the axis of symmetry for different Mach numbers obtained with RSPH: (—) 97,200 particles with $Ma = 0.05$, (- - -) 97,200 particles with $Ma = 0.1$, (-·-·-) 97,200 particles with $Ma = 0.025$.

Finally, we investigated the effect of the outflow boundary condition on the solution, by increasing the length of the computation domain to $L/B = 4$, while keeping all other parameters (e.g., particle resolution, Mach number) constant. The corresponding results of temperature, velocity and species mass fraction (not shown here for brevity) show very little difference between the two simulations.

The RSPH results are validated with numerical results obtained using a two-dimensional code [32] and the one-dimensional code OPPDIF [20]. The two-dimensional code is based on spectral element spatial discretization, and solves the low Mach form of the time dependent conservation equations of mass, momentum, energy and species. The integration is based on a high-order stiffly stable splitting scheme that couples the "hydrodynamic" (continuity and momentum) with the "thermo-chemistry" (species and energy) subsystems [32]. Detailed description of the numerical formulation and some applications can be found in [32–34]. OPPDIF is a one-dimensional model based on a similarity solution, with the introduction of a stream function [20]. All transport properties are computed the same way in all codes and the same kinetic scheme is employed.

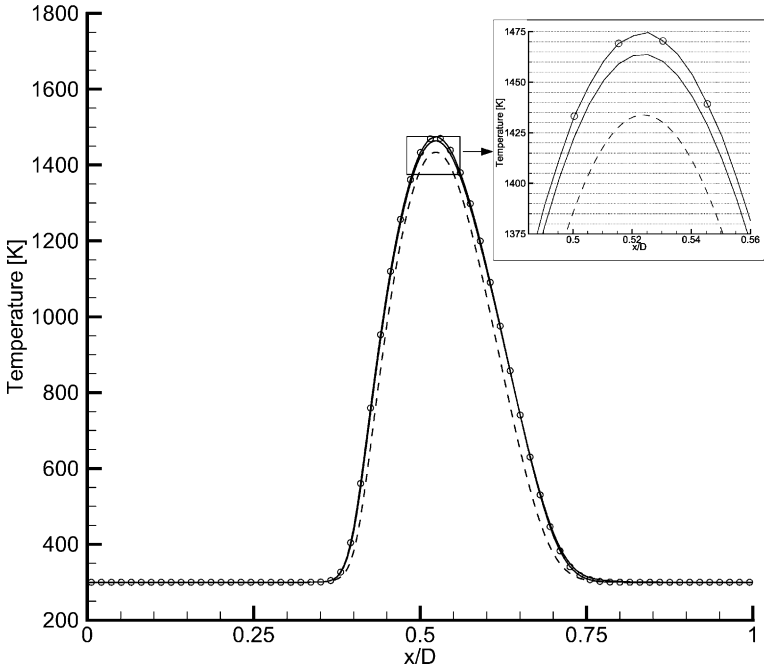

Fig. 9. Temperature profiles along the axis of symmetry. (—) RSPH simulation using 97,200 particles, (○) 2-D spectral element code simulation, (- - -) OPPDIF simulation.

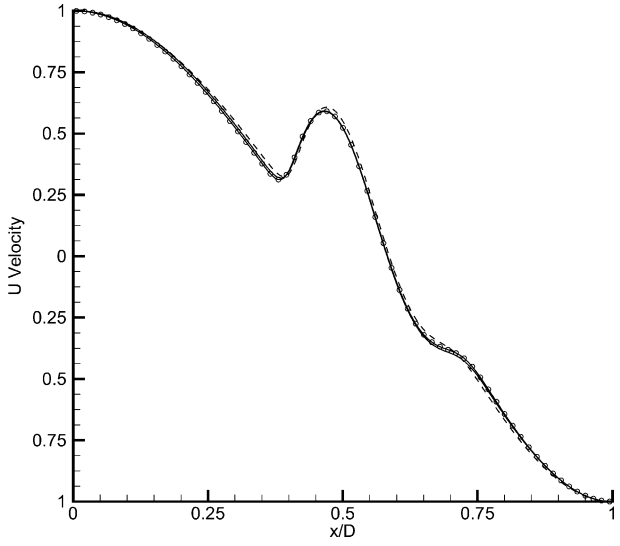

Fig. 10. Axial velocity profiles (non-dimensional) along the axis of symmetry. (—) RSPH simulation using 97,200 particles, (○) 2-D spectral element code simulation, (- - -) OPPDIF simulation.

A comparison of the RSPH results for the temperature along the axis of symmetry with the 2-D and the 1-D simulation results is presented in Fig. 9, showing very good agreement with the spectral-element code. The RSPH simulation is performed with 97,200 particles, and the spectral element simulation employs 176

elements with 12th order polynomials in each spatial direction. The flame location and flame thickness are identical. The one-dimensional results obtained from OPPDIF yield the same flame location, but smaller flame thickness and lower maximum temperature, by about 40 K (2.7%). As discussed in [33], this difference between the one- and two-dimensional simulations is due to two-dimensional effects.

The axial velocity profiles and the species profiles along the axis of symmetry are shown in Figs. 10 and 11, respectively. The agreement between the RSPH and the 2-D spectral element code is again very good, the difference for temperature, axial velocity and species being less than 1%. Very good agreement was observed not only along the axis of symmetry, but also in the remainder of the computational domain. This statement is exemplified and underpinned in Fig. 12 which shows the temperature, u-, v-velocities and characteristic species concentration profiles at distance $y = B$ away from the axis of symmetry, obtained with the RSPH and the spectral element code.

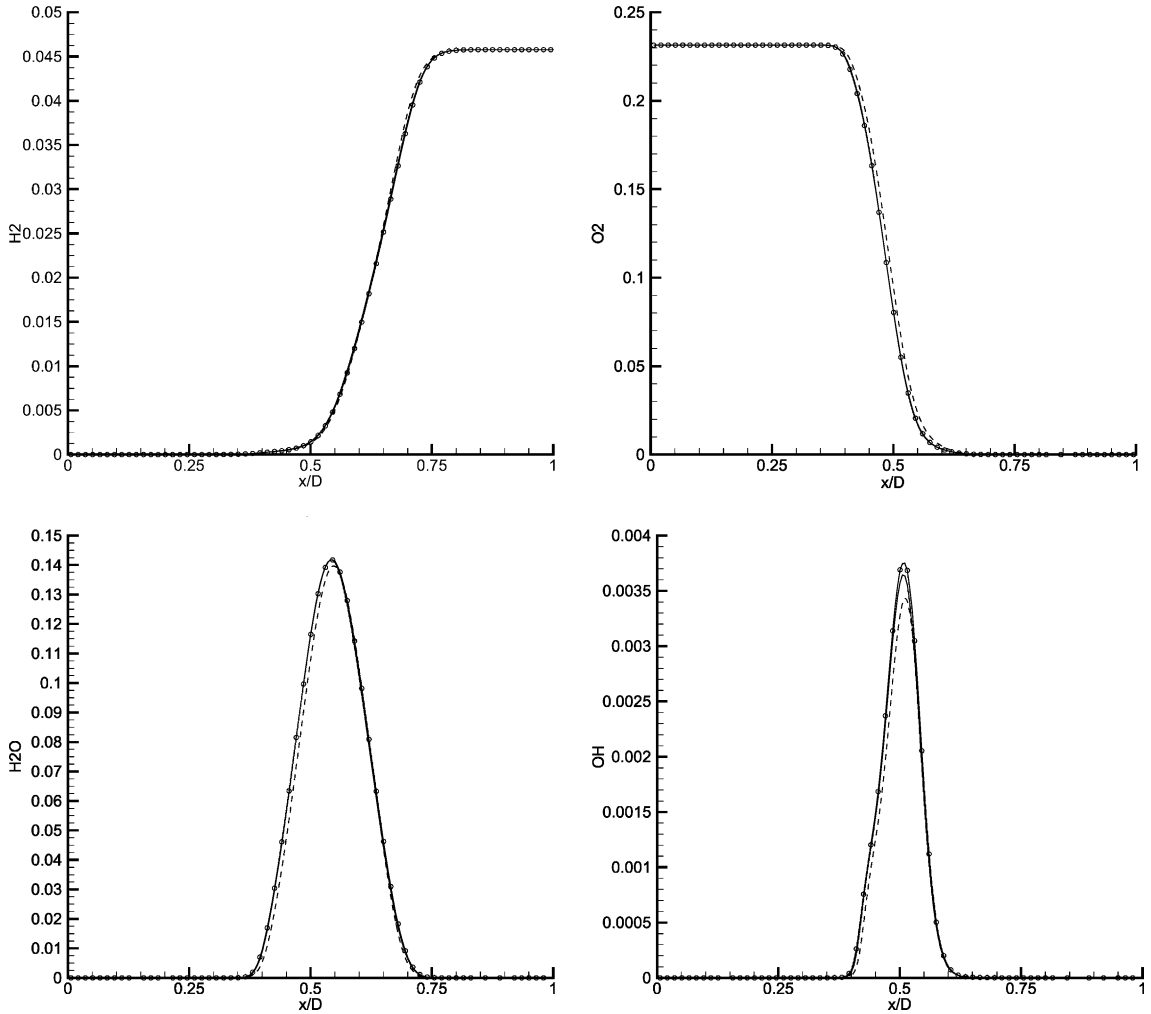

Fig. 11. Mass fraction profiles of H_2, O_2, H_2O and OH along the axis of symmetry. (—) RSPH simulation using 97,200 particles, (○) 2-D spectral element code simulation, (- - -) OPPDIF simulation.

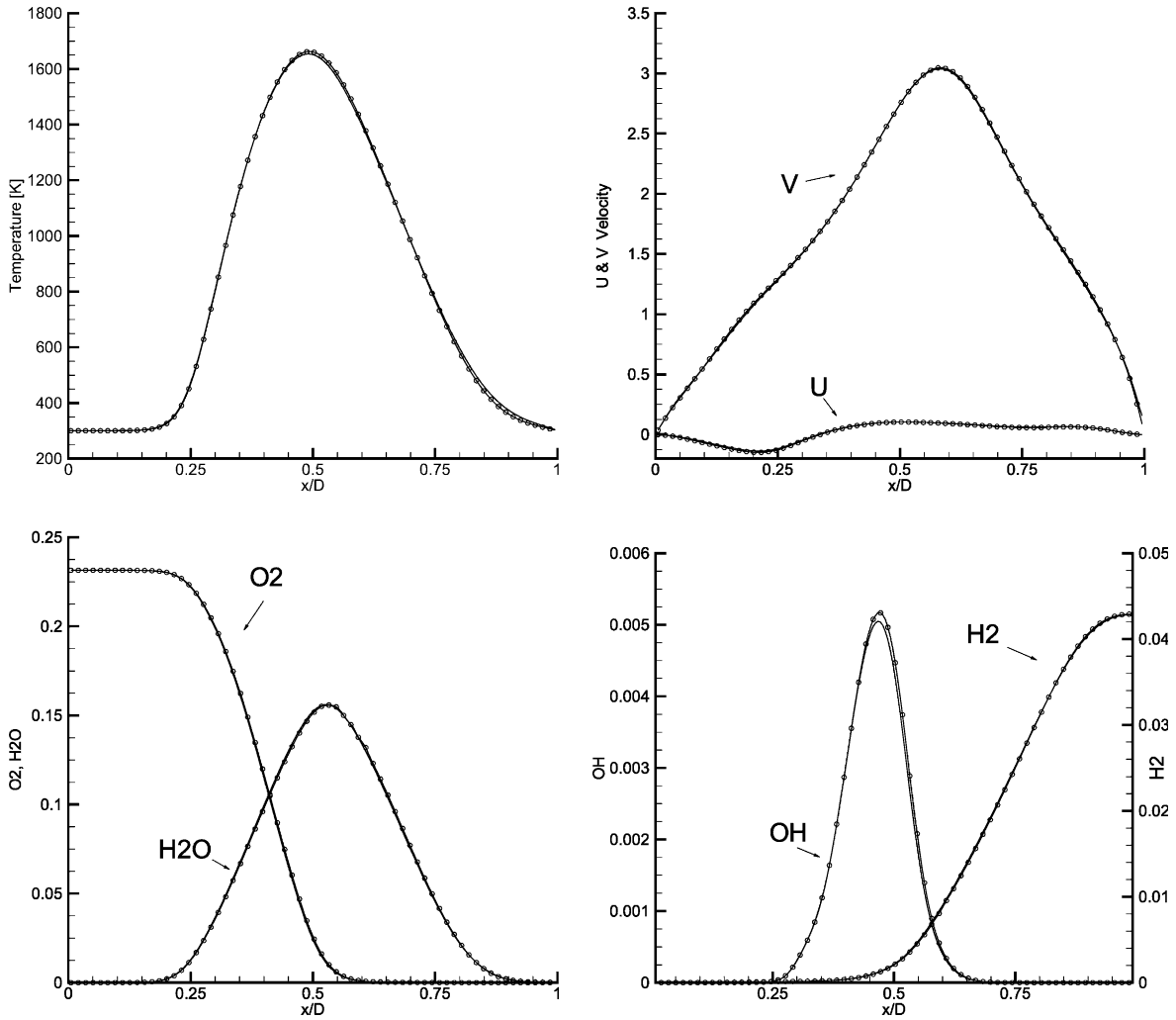

Fig. 12. Temperature, u and v velocity (non-dimensional) and mass fraction profiles at distance $y = 1.0B$ from the axis of symmetry. (—) RSPH simulation using 97,200 particles, (○) 2-D spectral element code simulation.

4. Conclusions

The RSPH methodology is extended to the simulation of chemically reacting flows and applied to the numerical modeling of a laminar, planar, opposed-jet burner. A detailed hydrogen-oxygen mechanism is used, involving nine species and 21 elementary reactions.

An extensive parametric study for the RSPH method is presented. In this study, the effect of particle resolution, Mach number, and length of the computational domain are investigated. In addition, the RSPH results are validated against the results obtained by a spectral element code. The excellent agreement indicates that RSPH is an accurate method for the simulation of reacting systems using detailed chemistry and transport. It should be pointed out, that there are no topological or geometrical assumptions in the RSPH scheme that can limit the applicability of the method in three dimensions. In addition, RSPH is

easily parallelizable (due to its nature as a particle method) and this is an inherent advantage of the technique compared to other methods. The results presented here were obtained with a code parallelized with a shared memory technique (OpenMP [35]). More sophisticated algorithms for distributed memory systems based on message-passing interface (MPI) can be used in SPH and RSPH. The best candidates for such parallelization are algorithms from molecular dynamics techniques (e.g. [36]).

Although not considered here, RSPH can be used to study flame-acoustic waves interaction [37] in compressible reacting flows, at least in the subsonic regime. One of the disadvantages of RSPH is the smearing of shock regions in highly compressible regions. Strong gradients (i.e., shocks and discontinuities) cannot be properly handled by the high order, moment conserving remeshing kernels we are currently using. Work is underway to circumvent this limitation by adopting special remeshing procedures that would accommodate relevant shock-capturing schemes while maintaining high order accuracy.

Acknowledgements

The Computing Center of the Swiss Federal Institute of Technology (ETHZ) and T. Racic are kindly acknowledged for providing support and computer time.

References

[1] T.J. Chung, Numerical Modeling in Combustion, Taylor and Francis, Washington, DC, 1993.
[2] T. Lappas, A. Leonard, P.E. Dimotakis, An adaptive Lagrangian method for computing 1-D reacting and nonreacting flows, J. Comput. Phys. 104 (1993) 361.
[3] A.F. Ghoniem, P. Givi, Lagrangian simulation of a reacting mixing layer at low heat release, AIAA J. 26 (1988) 690.
[4] A.F. Ghoniem, G. Heidarinejad, Effect of 2-dimensional shear-layer dynamics on mixing and combustion at low heat release, Combust. Sci. Technol. 72 (1990) 79.
[5] S. Yu, A random numerical-method with application in combustion, J. Comput. Math. 11 (1993) 113.
[6] P. Givi, Spectral and random vortex methods in turbulent reacting flows, in: F.A. Williams (Ed.), Turbulent Reacting Flows, Academic Press, London, England, 1994.
[7] A. Krishnan, A.F. Ghoniem, Simulation of rollup and mixing in Rayleigh–Taylor flow using the transport-element method, J. Comput. Phys. 99 (1992) 1.
[8] M.C. Soteriou, A.F. Ghoniem, Effects of the free-stream density ratio on free and forced spatially developing shear layers, Phys. Fluids 7 (1995) 2036.
[9] M.C. Soteriou, A.F. Ghoniem, Numerical Simulation of Unsteady Combustion Using the Transport Element Method, ESAIM Proceedings, (European Series in Applied and Industrial Mathematics), Montréal, Canada, 1996.
[10] C. Greengard, The core spreading vortex method approximates the wrong equation, J. Comput. Phys. 61 (1985) 345.
[11] F. Battaglia, P. Givi, Direct lagrangian simulations of a mixing layer by the transport-element method, J. Non-Equilib. Thermodyn. 18 (1993) 173.
[12] M.C. Soteriou, A.F. Ghoniem, On the effects of the inlet boundary condition on the mixing and burning in reacting shear flows, Combust. Flame 112 (1998) 404.
[13] P.J. O' Rourke, J.U. Brackbill, B. Larrouturou, On particle grid interpolation and calculating chemistry in particle-in-cell methods, J. Comput. Phys. 109 (1993) 37.
[14] G. Lapenta, J.U. Brackbill, Control of the number of particles in fluid and MHD particle-in-cell methods, Comput. Phys. Commun. 87 (1995) 139.
[15] A.K. Chaniotis, D. Poulikakos, P. Koumoutsakos, Remeshed smoothed particle hydrodynamics for the simulation of viscous and heat conducting flows, J. Comput. Phys. 182 (2002) 67.
[16] F.A. Williams, Combustion Theory, Benjamin/Cummings Publishing Company, Menlo Park, CA, 1985.
[17] K.K. Kuo, Principles of Combustion, Wiley, New York, 1986.
[18] R.J. Kee, G. Dixon-Lewis, J. Warnatz, M.E. Coltrin, J.A. Miller, A Fortran computer package for the evaluation of gas-phase, multicomponent transport properties. Report No. Sandia Report SAND86-8246, 1986.
[19] T.P. Coffee, J.M. Heimerl, Transport algorithms for premixed, laminar steady-state flames, Combust. Flame 43 (1981) 273.
[20] A.E. Lutz, R.J. Kee, J.F. Grcar, F.M. Rupley, OPPDIF: a Fortran program for computing opposed-flow diffusion flames. Report No. Sandia Report SAND96-8243, 1997.

[21] J.J. Monaghan, Particle methods for hydrodynamics, Comput. Phys. Rep. 3 (1985) 71.
[22] J.J. Monaghan, Smoothed particle hydrodynamics, Annu. Rev. Astron. Astrophys. 30 (1992) 543.
[23] J.P. Morris, P.J. Fox, Y. Zhu, Modeling low reynolds number incompressible flows using SPH, J. Comput. Phys. 136 (1997) 214.
[24] S.J. Watkins, A.S. Bhattal, N. Francis, J.A. Turner, A.P. Whitworth, A new prescription for viscosity in smoothed particle hydrodynamics, Astron. Astrophys. Suppl. Ser. 119 (1996) 177.
[25] P.W. Cleary, J.J. Monaghan, Conduction modelling using smoothed particle hydrodynamics, J. Comput. Phys. 148 (1999) 227.
[26] I.J. Schoenberg, Contribution to the problem of approximation of equidistant data by analytic functions, Quart. J. Appl. Math. 4 (1946) 45.
[27] P. Koumoutsakos, Inviscid axisymmetrization of an elliptical vortex, J. Comput. Phys. 138 (1997) 821.
[28] G.H. Cottet, P.D. Koumoutsakos, Vortex Methods: Theory and Practice, Cambridge University Press, Cambridge, London, 2000.
[29] T.J. Poinsot, S.K. Lele, Boundary-conditions for direct simulations of compressible viscous flows, J. Comput. Phys. 101 (1992) 104.
[30] G.D. Byrne, Pragmatic experiments with Krylov methods in the stiff ODE setting, in: I. Gladwell (Ed.), Computational Ordinary Differential Equations, Oxford University Press, Oxford, 1992.
[31] R.A. Yetter, F.L. Dryer, H. Rabitz, A comprehensive reaction-mechanism for carbon-monoxide hydrogen oxygen kinetics, Combust. Sci. Technol. 79 (1991) 97.
[32] A.G. Tomboulides, J.C. Lee, S.A. Orszag, Numerical simulation of low Mach number reactive flows, J. Sci. Comput. 12 (1997) 139.
[33] C.E. Frouzakis, J.C. Lee, A.G. Tomboulides, K. Boulouchos, Two-dimensional direct numerical simulation of opposed-jet hydrogen/air diffusion flame, Proc. Comb. Inst. 27 (1998) 571.
[34] C.E. Frouzakis, A.G. Tomboulides, J. Lee, K. Boulouchos, From diffusion to premixed flames in an H-2/air opposed-jet burner: the role of edge flames, Combust. Flame 130 (2002) 171.
[35] HP, Parallel Programming Guide for HP-UX Systems, Document Number: B3909-90008, HP-ux 11i version 1.5, 2001.
[36] S. Plimpton, Fast parallel algorithms for short-range molecular-dynamics, J. Comput. Phys. 117 (1995) 1.
[37] M. Gonzalez, Acoustic instability of a premixed flame propagating in a tube, Combust. Flame 107 (1996) 245.